Available online at www.sciencedirect.com

SCIENCE DIRECT®

Earth and Planetary Science Letters 235 (2005) 79–95

EPSL

www.elsevier.com/locate/epsl

In situ benthic fluxes from an intermittently active mud volcano at the Costa Rica convergent margin

P. Linke[a,*], K. Wallmann[a,1], E. Suess[a,2], C. Hensen[b,3], G. Rehder[a,4]

[a] *IFM-GEOMAR, Leibniz-Institut für Meereswissenschaften, Dienstgebäude Ostufer, Wischhofstr. 1-3, 24148 Kiel, Germany*
[b] *Sonderforschungsbereich 574, Christian-Albrechts-Universität zu Kiel, Wischhofstr. 1-3, 24148 Kiel, Germany*

Received 20 July 2004; received in revised form 17 February 2005; accepted 11 March 2005
Available online 23 May 2005
Editor: E. Boyle

Abstract

Along the erosive convergent margin off Costa Rica a large number of mound-shaped structures exist built by mud diapirism or mud volcanism. One of these, Mound 12, an intermittently active mud volcano, currently emits large amounts of aqueous dissolved species and water. Chemosynthetic vent communities, authigenic carbonates, and methane plumes in the water column are manifestations of that activity. Benthic flux measurements were obtained by a video-guided Benthic Chamber Lander (BCL) deployed at a vent site located in the most active part of Mound 12. The lander was equipped with 4 independent chambers covering adjacent areas of the seafloor. Benthic fluxes were recorded by repeated sampling of the enclosed bottom waters while the underlying surface sediments were recovered with the lander after a deployment time of one day. One of the chambers was placed directly in the centre of an active vent marked by the occurrence of a bacterial mat while the other chambers were located at the fringe of the same vent system at a lateral distance of only 40 cm. A transport-reaction model was developed and applied to describe the concentration profiles in the pore water of the recovered surface sediments and the temporal evolution of the enclosed bottom water. Repeated model runs revealed that the best fit to the pore water and benthic chamber data is obtained with a flow velocity of 10 cm yr^{-1} at the centre of the vent. The flux rates to the bottom water are strongly modified by the benthic turnover (benthic filter). The methane flux from below at the bacterial mat site is as high as 1032 μmol cm^{-2} yr^{-1}, out of which 588 μmol cm^{-2} yr^{-1} is oxidised in the surface sediments by microbial consortia using sulphate as terminal electron acceptor and 440 μmol cm^{-2} yr^{-1} are seeping into the overlaying bottom water. Sulphide is transported to the surface by ascending fluids (238 μmol cm^{-2} yr^{-1}) and is formed within the surface sediment by the anaerobic oxidation of methane (AOM, 588 μmol cm^{-2} yr^{-1}). However,

* Corresponding author. Tel.: +49 431 600 2115; fax: +49 431 600 2911.
E-mail addresses: plinke@ifm-geomar.de (P. Linke), kwallmann@ifm-geomar.de (K. Wallmann), esuess@ifm-geomar.de (E. Suess), chensen@ifm-geomar.de (C. Hensen), grehder@ifm-geomar.de (G. Rehder).
[1] Tel.: +49 431 600 2287; fax: +49 431 600 2829.
[2] Tel.: +49 431 600 2232; fax: +49 431 600 2829.
[3] Tel.: +49 431 600 2567; fax: +49 431 600 2916.
[4] Tel.: +49 431 600 2283; fax: +49 431 600 2829.

0012-821X/$ - see front matter
doi:10.1016/j.epsl.2005.03.009

sulphide is not released into the bottom water but completely oxidized by oxygen and nitrate at the sediment/water interface. The oxygen and nitrate fluxes into the sediment are high (781 and 700 μmol cm^{-2} yr^{-1}, respectively) and are mainly driven by the microbial oxidation of sulphide. Benthic fluxes were much lower in the other chambers placed in the fringe of the vent system. Thus, methane and oxygen fluxes of only 28 and 89 μmol cm^{-2} yr^{-1}, respectively were recorded in one of these chambers. Our study shows that the aerobic oxidation of methane is much less efficient than the anaerobic oxidation of methane so that methane which is not oxidized within the sediment by AOM is almost completely released into the bottom water. Hence, anaerobic rather than aerobic methane oxidation plays the major role in the regulation of benthic methane fluxes. Moreover, we demonstrate that methane and oxygen fluxes at cold vent sites may vary up to 3 orders of magnitude over a lateral distance of only 40 cm indicating an extreme focussing of fluid flow and methane release at the seafloor.

Keywords: benthic fluxes; methane; mud volcano; Costa Rica margin

1. Introduction

Active convergent margins are important regions for element recycling between crust, ocean and atmosphere [1]. The input into subduction zones is by sediments and altered oceanic crust and the return flow of volatile elements may take three transport pathways: through the subduction zone vents at the deformation front, the mud diapirs at the mid slope, and through subarial volcanoes at the arc. Mass transport through mud diapirism by ascending muds and fluids is being increasingly recognized as a potentially important, but largely unquantified process [2,3]. For example, the Mariana fore-arc serpentinite mud diapirs are spectacular features, that transport fluids and material from up to 50 km of depth to the surface [4]. Other well-known subduction-related mud diapirs are found off the Indonesian island arc, Barbados, Costa Rica, Pakistan, and on the Mediterranean Ridge (e.g. [5–8]). Mud diapirs at the erosive margin off Costa Rica have been known from extensive surveys previous to ODP Leg 170 which included a seismic [9] and an *Alvin* diving program [10,11]. More recently, numerous geophysical and mapping surveys combined with video observations revealed a great number of mud diapirs at mid slope depths between 1000 to 3000 m [12,13], five of which have been studied in detail so far [14–17].

This study aimed at establishing benthic fluxes from one of these mounds, Mound 12, located in ~1000 m water depth on the mid slope off Costa Rica (Figs. 1 and 2). It is essentially round with a diameter of 800 m and features an irregular higher pinnacle at its NE end and a lower profile ridge towards the SW [18]. A widespread occurrence of chaotic mud flows interlayered with stratified slope sediments indicate frequent mud eruptions that alternate with periods of quiescence when only fluid venting occurs [18]. Video surveys revealed that the pinnacle top and its SW flank are partially covered with authigenic carbonates and typical cold vent fauna communities (Mytilid mussels, pogonophoran tubeworms and bacterial mats) [15,17]. These indicators suggest strong venting activity which is supported by the highest bottom water methane concentrations of all surveyed mounds at Mound 12 (>30 times the regional background of 1–2 nmol/l) [17].

During Meteor cruise M54/3a we obtained data from video-guided deployments of a Benthic Chamber Lander and a Multiple Corer, as well as by recovering standard gravity cores to evaluate the role of the benthic filter to the flux into the bottom water at Mound 12. To our knowledge this is the first integrative study encompassing pore water and sediment–water interface data, aimed at quantifying the in situ fluid flow and benthic turnover at a vent site. The interrelationship between pore water chemistry, biological activity, and production rates of mud and fluid is crucial for our understanding of vent systems at active margins. On one hand, the development of chemoautotrophic microbial and symbiotic communities is dependent on the transfer rates of reduced inorganic substrates [19,20], and on the other hand this mass transfer is modified and

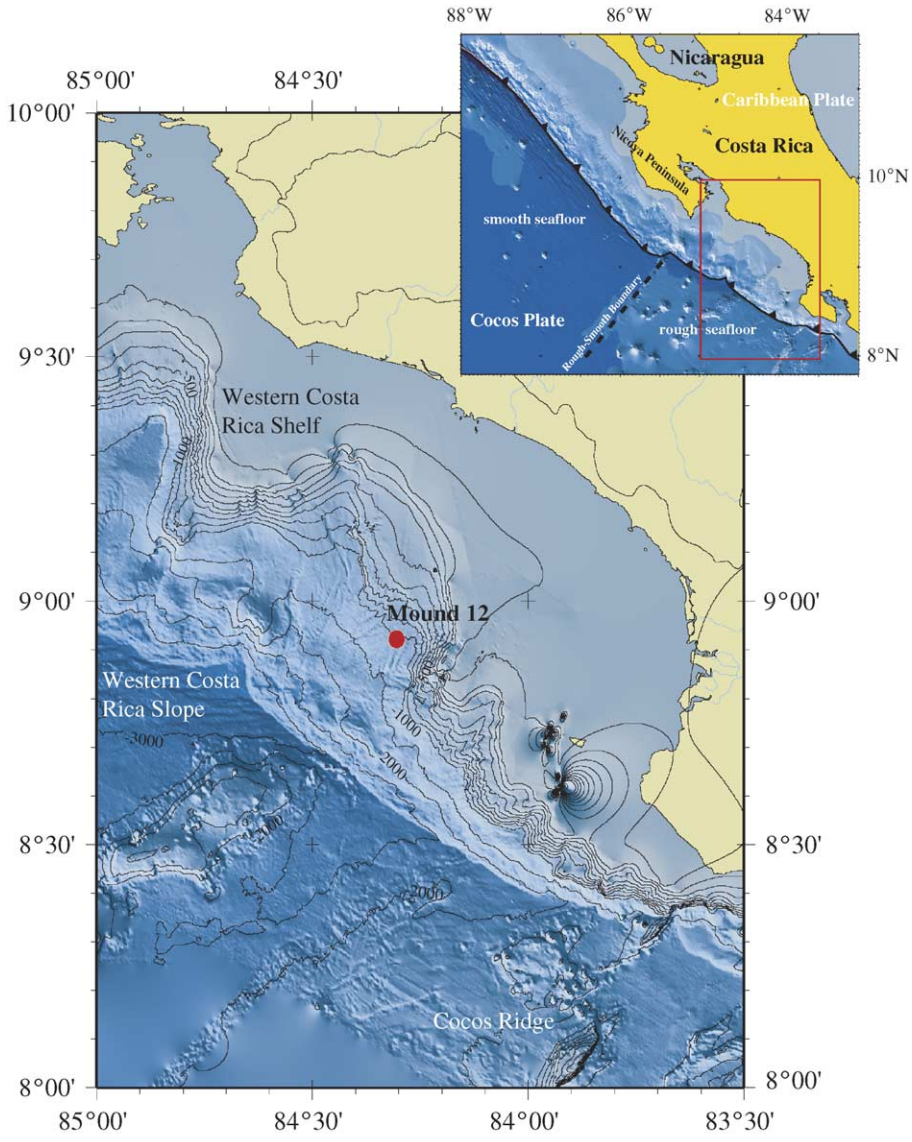

Fig. 1. Bathymetry of the SFB 574-research area showing the Middle American subduction zone, the rough and smooth topography of the oceanic crust, and the location of Mound 12 located in ~1000 m water depth at the mid slope off Costa Rica.

filtered by their activities. Therefore, aqueous flow rates, the controlling parameters of fluid expulsion and resulting transient flow patterns, the concentrations of methane and reduced sulfur compounds delivered by the aqueous flow, and their transformation rates are important parameters for the determination of mass balances in various subduction zone settings.

2. Instruments and methods

2.1. Benthic lander deployment

In situ flux measurements were performed at Mound 12 with the *B*enthic *C*hamber *L*ander (BCL) [21]. The basic frame of the lander is a stainless-steel tripod that carries 21 Benthos glass spheres for

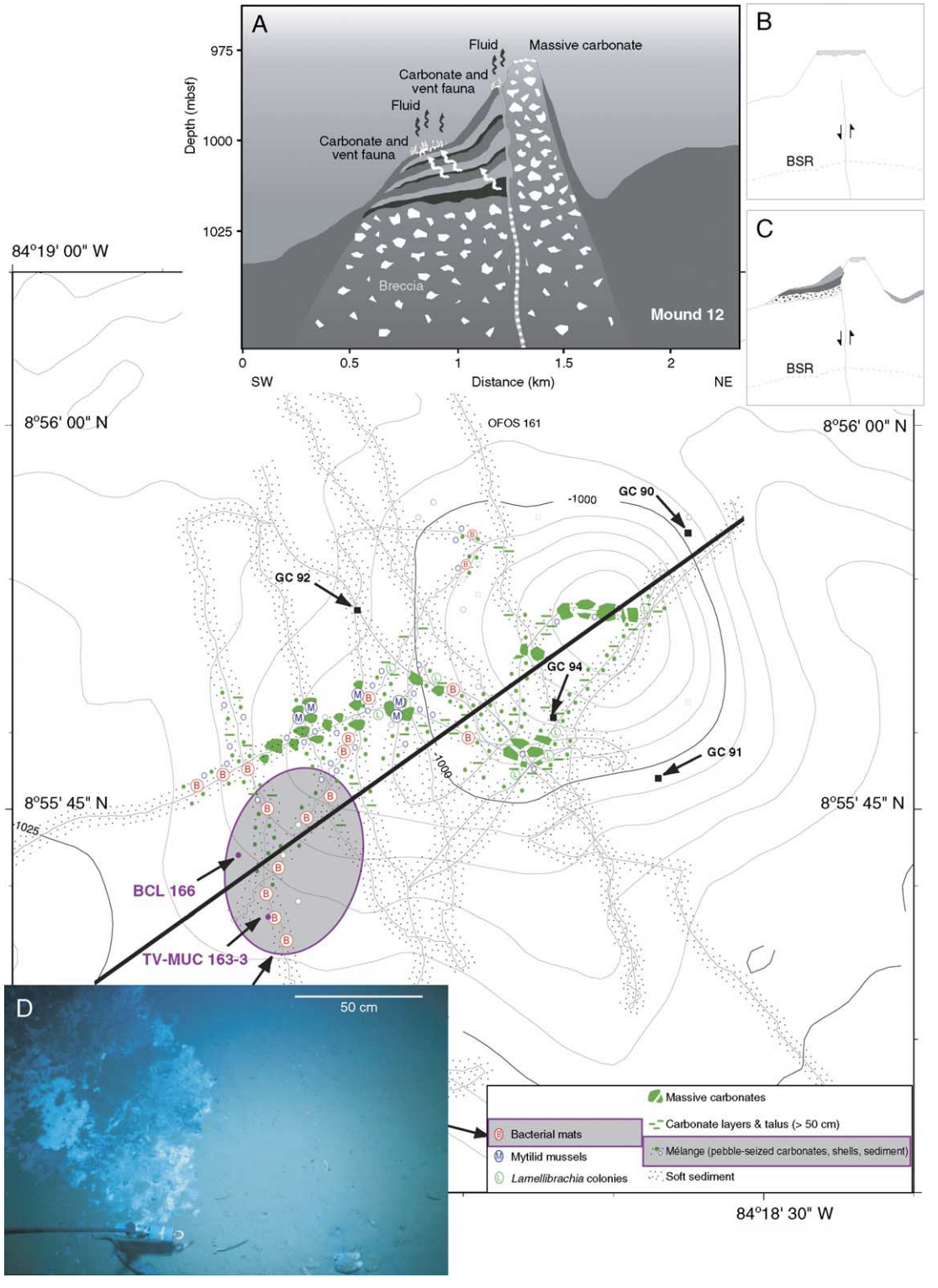
A
Fluid
Massive carbonate
Carbonate and vent fauna
Fluid
Carbonate and vent fauna
Breccia
Mound 12
Depth (mbsf)
975
1000
1025
0
0.5
1
1.5
2
SW
Distance (km)
NE
B
BSR
C
BSR
84°19' 00" W
8°56' 00" N
OFOS 161
-1000
GC 90
GC 92
GC 94
GC 91
8°55' 45" N
1025
BCL 166
TV-MUC 163-3
D
50 cm
Massive carbonates
Bacterial mats
Carbonate layers & talus (> 50 cm)
Mytilid mussels
Mélange (pebble-seized carbonates, shells, sediment)
Lamellibrachia colonies
Soft sediment
84°18' 30" W

buoyancy and ballast attached by release toggles to each leg. The ballast is controlled by two acoustic release units that provide redundancy. A radio beacon and strobe aid in location and recovery at the surface and an ARGOS system is used to track the lander in case of a premature release. The frame was equipped with four cube-shaped Delrin chambers ($20 \times 20 \times 26$ cm) sitting in a stainless-steel frame which is attached to the lander. Each benthic chamber is an autonomous module with control unit and power supply by rechargeable NiCd-battery packs (6 V, 10 A h) integrated in a Benthos glass sphere.

The BCL was deployed with a video-guided launcher connected to the ship's coaxial cable [22] at a site covered by white patches of bacterial mats (station 166, Fig. 2) indicative of rapid discharge of reduced components from the sediments. Two hours after deployment, the chambers were driven slowly into the sediment by a motor in order to allow any resuspension to be swept away and/or settled out. After the chambers were in place their lids, which carry a central stirrer, were closed. During each incubation, sequential samples are collected with syringe water samplers attached to each chamber. The BCL is equipped with seven glass syringes which obtain water samples of 50 ml each at pre-set intervals from the water inside the incubation chamber. The volume drawn by each syringe is replaced by ambient bottom water. The total incubation time, calculated from first-to-last syringe sampling was 26.5 h. At the end of each incubation period a shutter at the bottom was drawn by a second motor to retrieve the incubated sediment. Once the shutter was closed the chamber was slowly heaved out of the sediment by the first motor and the lander was ready for recovery. The depth of the sediment retrieved and the height of the overlying water were measured after recovery of the BCL to determine the volume of the enclosed water.

2.2. Pore water sampling

After recovery of the BCL push corers were taken to subsample the sediments retrieved from Mound 12. Two of the four benthic chambers yielded push cores for subsampling at depth intervals between 1 and 2 cm.

In order to characterize the pore water environment at Mound 12 and to supplement the data from the BCL deployment we collected one video-guided Multiple Corer (TV-MUC 163-3) near the site of the BCL deployment (Fig. 2), and four standard gravity cores covering Mound 12 (GC-90, -91, -92, -94).

At gravity core locations where methane was expected to be present, syringe samples were taken on deck from every cut segment surface. All TV-MUC cores were immediately placed in a cooling room and processed at about 4 °C. Supernatant bottom water of the TV-MUC cores was sampled and filtered for subsequent analyses. The TV-MUC core was processed immediately after recovery and sub-samples for methane analyses were taken. Push cores and the TV-MUC core were cut into slices for pressure filtration with a minimum depth resolution of 0.5 cm. Gravity cores were cut lengthwise after recovery. On the working halves pH was determined with an electrode and sample intervals between 10–50 cm were taken for pressure filtration with Teflon- and PE-squeezers. The squeezers were operated with argon at a pressure gradually increasing up to 5 bar. Depending on the porosity and compressibility of the sediments, up to 30 ml of pore water were retrieved from each sample through 0.2 μm cellulose acetate membrane filters.

2.3. Analytical techniques

2.3.1. Lander samples

Oxygen concentrations were determined by two replicate Winckler titrations of each syringe water sample when sufficient volume was available.

Fig. 2. Detailed bathymetric map of Mound 12 showing the sampled locations, tracks and interpretations from video sled deployments (modified from [17]); contour intervals: 5 m. Inserted is a conceptual model of Mound 12. (A) Schematic cross-section (SW-NE, thick black line in map) through the fault controlled mud volcano and the older pinnacle in the NE. (B,C) Failure of the seaward half, formation of a basal carbonate and shell debris subsequently covered by mud flows and hemipelagic sediments (figures modified from [18]). (D) The underwater photograph documents the present colonisation of the vent sediment by bacterial mats together with pebble-sized carbonates and clam shells at the deployment site of the lander (BCL 166) and TV-MUC 163-3 in the SW of Mound 12 (shaded area).

Methane concentrations were analysed by adding 12 ml of water from the syringe sampler to 1.5 g of NaCl into 24 ml septum vials. The crimp cap vials were closed and shaken for several minutes to allow complete dissolution of the salt and transfer of the dissolved gases into the headspace. The methane mole fraction in the headspace was determined by injecting a sample of the gas into a Shimadzu GC 14 A GC equipped with an FID and a 4 m 1/8′ Poraplot Q (mesh 50/80) packed column. Three blanks were analysed by injecting water previously degassed under vacuum. The blank basically is introduced by the air phase with an atmospheric mole fraction of 1.8 ppm V. Methane concentrations of the water were calculated from the mole fraction of methane in the headspace gas according to the equation:

$$C_w = (X_{mes} - X_{blank}) \cdot V_g \cdot (1000/V_w)/22.38 \quad (1)$$

where C_w is the methane concentration in the water in nmol/l, X_{mes} and X_{blank} are the mole fractions of the gas in the sample headspace and the gas, and V_w and V_g are the volumes of the injected water sample and the gas head space, respectively [23].

2.3.2. Methane in bulk sediment

Three milliliters of sediment were injected into 24 ml septum vials containing 9 ml of a concentrated NaCl-solution. After closing and subsequent shaking methane becomes enriched in the headspace of the vial. The methane content of the headspace was analysed with the gas chromatographic system described above. One replicate was taken and poisoned with a saturated NaOH solution for subsequent isotopic analyses.

2.3.3. Pore water

Pore water analysis of the following parameters was carried out on board: nitrate, ammonia, phosphate, alkalinity, hydrogen sulfide, chloride, methane, silicate, calcium, and pH. Modifications of some methods were necessary for samples with high sulfide concentrations. Detailed descriptions of the methods are available on http://www.ifm-geomar.de/index.php?id=1858&L=1.

Nitrate and phosphate were measured photometrically using standard methods described by Grasshoff and Anderson [24]. Samples of the sediment pore water were analysed for total alkalinity by titration of 0.5–1 ml pore water according to Ivanenkov and Lyakhin [25]. During titration the sample was degassed by continuously bubbling nitrogen to remove the generated CO_2 or H_2S. The acid was standardized against IAPSO (International Association for the Physical Sciences of the Oceans) standard seawater. The Grasshoff and Anderson [24] method for sulfide determination was adapted for pore water concentrations of dissolved sulfide in the range of millimolar amounts. For reliable and reproducible results, an aliquot of pore water was diluted with appropriate amounts of oxygen-free artificial seawater; the sulfide was fixed by immediate addition of zinc acetate gelatin solution immediately after pore water recovery. After dilution, the sulfide concentration in the sample should be less than 50 μmol/l. Chloride was determined by titration with $AgNO_3$ standardized against IAPSO standard seawater. To prevent interferences with high concentrations of H_2S (>1 mM) these samples were pre-treated with a 1:1 dilution of 0.01 N suprapure HNO_3 and stored for 1–2 days, without lid, in a cool room. Dissolved sulfate was determined using ion-chromatography (Sykam, conductivity detector S3110) with sodium bicarbonate as solvent.

Shore-based determinations included dissolved element concentrations (Ca, Mn, Ba) on acidified sub-samples using optical ICP. Porosity was calculated from the weight loss of wet sediment subsamples upon freeze-drying.

2.4. Numerical transport-reaction model

A transport-reaction model was used to simulate the concentration profiles in the pore water and the changes in bottom water composition inside the benthic chamber. The software package MATHEMATICA version 4.2 was used to implement the model and MATHEMATICA's NDSolve object was applied for the numerical integration of the different equations. NDSolve uses the Method-of-lines code for integration, a finite difference procedure which has been frequently applied in the modelling of early diagenetic processes [26–29].

2.4.1. Pore water

The vertical distribution of dissolved methane, sulfate and sulfide in sediment pore waters affected

by upward flow of a methane-charged fluid may be described by the following partial differential equation:

$$\frac{\delta C}{\delta t} = \frac{1}{\delta x} \cdot \left(\Phi \cdot \frac{D_M}{\Theta^2} \cdot \frac{\delta C}{\delta x} + \Phi \cdot v_s \cdot C \right) + \Phi \cdot R_{AOM} \tag{2}$$

where C is the dissolved species concentration in sediment pore water, t is time, x is sediment depth, Φ is porosity, Θ is sediment tortuosity, D_M is the molecular diffusion coefficient, v_S is the rate of vertical fluid ascend in porous sediments and R_{AOM} is the rate of anaerobic oxidation of methane. Bioirrigation was not included since no macrofauna was observed in the cores used for modelling.

Fluid flow and sediment tortuosity depend on porosity as follows [30]:

$$v_s = \frac{v_0 \cdot \Phi_0}{\Phi} \qquad \Theta^2 = 1 - \ln\left(\Phi^2\right) \tag{3}$$

where v_0 and Φ_0 are fluid flow velocity and porosity at zero depth. Porosity decreases exponentially with depth so that v_S, Θ, and Φ are not constant parameters but functions of x.

In vent environments, the turnover of sulfide, methane and sulfate is controlled mainly by the anaerobic oxidation of methane [28,31,32]. The different species are affected according to the overall stoichiometry of the AOM reaction:

$$CH_4 + SO_4^{2-} \Rightarrow HCO_3^- + HS^- + H_2O. \tag{4}$$

Thus, sulfate and methane are consumed while sulfide is produced via AOM. The AOM rate (R_{AOM}) is proportional to the dissolved methane concentration and is limited by the availability of sulfate [29]:

$$R_{AOM} = k_{AOM} \cdot C_{CH4} \cdot \left(\frac{C_{SO4}}{C_{SO4} + K_{SO4}} \right) \tag{5}$$

where k_{AOM} is a kinetic constant, C_{CH4} and C_{SO4} are the concentrations of dissolved methane and sulfate, respectively, and K_{SO4} is a Monod constant (K_{SO4}=2 mM). We used a Monod formulation rather than bimolecular kinetics because experimental data show that sulfate has no significant effect on the AOM rate as long as sulfate concentrations are greater than 2 mM ([29], and personal communication K. Nauhaus).

2.4.2. Boundary conditions

Marine sediments are subject to rapidly flowing turbulent bottom waters. Very close above the sediment surface, lateral water flow and eddy diffusion are strongly diminished so that diffusive processes dominate the vertical solute transport. This so-called "diffusive boundary layer" extends typically about 1 mm into the overlying bottom water [30]. In a vent setting with slow vertical fluid flow, the vertical distribution of an inert tracer in this almost stagnant layer may be calculated from the following steady-state differential equation:

$$D_M \cdot \frac{\delta^2 C}{\delta x^2} + v \cdot \frac{\delta C}{\delta x} = 0 \tag{6}$$

The equation can be scaled to the layer thickness zd and divided by D_M to obtain:

$$\frac{\delta^2 C}{\delta z^2} + Pe \cdot \frac{\delta C}{\delta z} = 0 \qquad z = \frac{x}{zd} \qquad Pe = \frac{v \cdot zd}{D_M} \tag{7}$$

where Pe is a non-dimensional Peclet number [30]. The transport in the boundary layer is dominated by molecular diffusion if Pe is smaller than unity. Inserting realistic values for D_M (300 $cm^2\ yr^{-1}$) and zd (0.1 cm), the condition $Pe<1$ is obeyed as long as the vertical flow velocity is smaller than about 2000 $cm\ yr^{-1}$. At cold vent sites, the vertical fluid flow velocity typically falls into a range of 0–1000 $cm\ yr^{-1}$. Thus, the diffusive transport of dissolved species through a boundary layer of approximately 0.1 cm thickness controls the transfer of chemicals into the overlying water column not only in ordinary seafloor settings but also at cold vent sites.

The fluxes of dissolved species at the sediment–water interface (at $x=0$) are thus defined by the following equation which is also used as upper boundary condition for the modeling of pore water profiles:

$$\Phi(0) \cdot \left(\frac{D_M}{\Theta^2(0)} \cdot \left. \frac{\delta C}{\delta x} \right|_{x=0} + v \cdot C(0) \right) = D_M \cdot \frac{C(0) - C_{BW}}{zd} \tag{8}$$

where $\Phi(0)$and $\Theta(0)$ are sediment porosity and tortuosity at zero depth, $C(0)$ is the concentration

at the sediment–water interface, and C_{BW} is the concentration prevailing in the overlying bottom water. The interface concentration $C(0)$ is calculated in the sediment model. For sulfate, $C(0)$ is smaller than C_{BW} because sulfate is consumed in the sediment column while $C(0)$ values for sulfide and methane are greater than the corresponding C_{BW} values. Direction and magnitude of the diffusive flux across the sediment–water interface are defined by the difference between $C(0)$ and C_{BW} values.

At the base of the sediment column, concentrations are determined by the composition of the rising vent fluids. Thus, concentrations are set to constant values at the lower boundary.

2.4.3. Concentrations in the flux chamber of the BCL

Changes in dissolved sulfide and methane in the enclosed bottom water are controlled by the benthic release of these reduced species and the oxidation via oxygen and nitrate (R_{OX}). The temporal changes in concentration can be described by a set of ordinary differential equations:

$$\frac{\delta C_{CH}}{\delta t} = \frac{A_{CH}}{V_{CH}} \cdot D_M \cdot \frac{C(0) - C_{CH}}{zd} - \sum s_{OX} \cdot R_{OX} \quad (9)$$

where A_{CH} is the seafloor area covered by the benthic chamber, V_{CH} is the chamber volume, C_{CH} is the time-dependent concentration of methane or sulfide in the bottom chamber whereas $C(0)$ coincides with the concentration at zero depth calculated in the pore water model. The stoichiometric coefficients (s_{OX}) are derived from the overall stoichiometry of the oxidation reactions defined as:

Aerobic sulfide oxidation:

$$HS^- + 2O_2 \Rightarrow SO_4^{2-} + H^+ \quad (10)$$

Table 1
Parameter values used in the modeling

Fixed parameters	Symbol	Value
Temperature[a]	T	4.5 °C
Seafloor areas covered by the benthic chamber[b]	A_{CH}	400 cm^2
Water volume in the benthic chamber[b]	V_{CH}	5600 cm^3
Porosity at zero depth[c]	Φ_0	0.81
Porosity at infinite depth[c]	Φ_f	0.73
Attenuation coefficient for porosity decrease with depth[c]	p	0.1 yr^{-1}
Molecular diffusion coefficient of sulfate[d]	$D_M^{SO_4}$	187 $cm^2\ yr^{-1}$
Molecular diffusion coefficient of bisulfide[d]	D_M^{HS}	367 $cm^2\ yr^{-1}$
Molecular diffusion coefficient of methane[d]	$D_M^{CH_4}$	337 $cm^2\ yr^{-1}$
Thickness of the diffusive boundary layer[e]	zd	0.04 cm
Data ranges used in the iterative model	**Symbol**	**Value**
Velocity of upward fluid flow at zero depth[f]	v_0	0–1000 (10) cm yr^{-1}
Methane concentration at the base of the model column[f]	$C_L^{CH_4}$	1–100 (40) mM
Kinetic constant for the anaerobic oxidation of methane[f]	k_{AOM}	0–100 (3) yr^{-1}
Kinetic constant for the aerobic oxidation of methane[f]	k_{OM}	10–10^8 (10^4) $mM^{-1}\ yr^{-1}$
Kinetic constant for the aerobic oxidation of sulfide[f]	k_{OS}	10–10^8 (10^7) $mM^{-1}\ yr^{-1}$
Kinetic constant for the oxidation of sulfide with nitrate[f]	k_{NS}	10–10^8 (10^7) $mM^{-1}\ yr^{-1}$

A range of values is given for each of the parameters which were varied during the fitting procedure. The values in parentheses produced the best fit to the data represented by the standard case.

[a] Measured by a CTD attached to the BCL.

[b] Determined from chamber geometry and penetration.

[c] Obtained by fitting an exponential equation (Porosity = $\Phi_f + (\Phi_0 - \Phi_f)$ exp(− p depth)) to the measured porosity depth profile.

[d] Calculated from equations given in [30] considering the ambient bottom water temperature of 4.5 °C.

[e] Literature value [21].

[f] Determined by fitting the model to pore water and chamber data.

Sulfide oxidation via nitrate:

$$HS^- + 8/5NO_3^- + 3/5H^+ \Rightarrow SO_4^{2-} + 4/5H_2O \quad (11)$$

Aerobic methane oxidation:

$$CH_4 + 2O_2 \Rightarrow CO_2 + 2H_2O. \quad (12)$$

The oxidation reactions occur mainly within the bacterial mat covering the surface sediments. The model does not resolve the complex transport pathways and biogeochemical processes occurring in the mat but simply relates the oxidation rates to the concentrations in the benthic chamber. Thus, the differential equations for oxygen and nitrate are defined as:

$$\frac{\delta C_{CH}}{\delta t} = -\sum s_{OX} \cdot R_{OX} \quad (13)$$

where the rate laws of the oxidation reactions (R_{OX}) follow bi-molecular kinetics:

Aerobic sulfide oxidation:

$$R_{OS} = k_{OS}[O_2][TH_2S] \quad (14)$$

Sulfide oxidation via nitrate:

$$R_{NS} = k_{NS}[NO_3][TH_2S] \quad (15)$$

Aerobic methane oxidation:

$$R_{OM} = k_{OM}[O_2][CH_4]. \quad (16)$$

At time zero, all concentrations are set equal to the bottom water concentration measured prior to the lander deployment (C_{BW}).

2.4.4. Modeling procedure

As a first step, the model is fitted to the pore water sulfate and sulfide data by varying the concentrations of methane in the rising fluids, the fluid advection rate and the kinetic constant for AOM (k_{AOM}). For this purpose, the system of three partial differential equations (Eq. (2)) is solved and run repeatedly until a good fit is obtained after reaching steady state.

Subsequently, the system of four ordinary differential equations describing the concentration changes of oxygen, nitrate, sulfide and methane in the benthic chamber is solved (Eqs. (9) and (13)) using the concentrations of sulfide and methane at zero depth determined in the previous runs of the pore water model. In these simulations the diffusive fluxes of sulfide and methane into the bottom water decrease over time due to the increasing concentrations in the chamber water (C_{CH}). The changes in concentration at zero depth ($C(0)$) are neglected because the pore water profiles remain almost unchanged over the very brief period of the lander deployment. The model was run repeatedly applying different parameter values until the model curves reproduced the concentrations measured in the pore water and the benthic chamber. The best fit to the data was obtained with the set of parameter values given in Table 1. The corresponding model run is referred to as standard case or standard run in the following assessment.

3. Results and discussion

3.1. Pore water composition

Pore fluids below bacterial mats have a strongly reducing character with high concentrations of dissolved sulfide, methane, barium and enhanced total

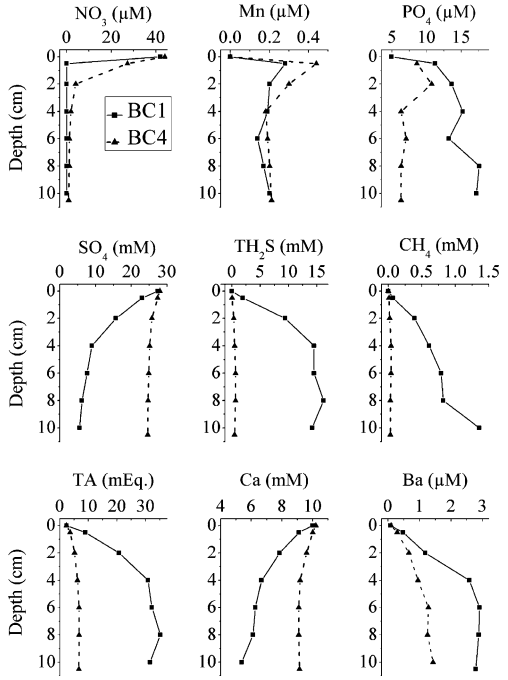

Fig. 3. Pore water composition in surface sediments recovered by 2 benthic chambers of BCL 166 which reveal an extreme heterogeneity of benthic fluxes over a lateral distance of only 40 cm. Whereas the sediment of Chamber 1 was completely covered by bacterial mats, Chamber 4 showed a slight coverage.

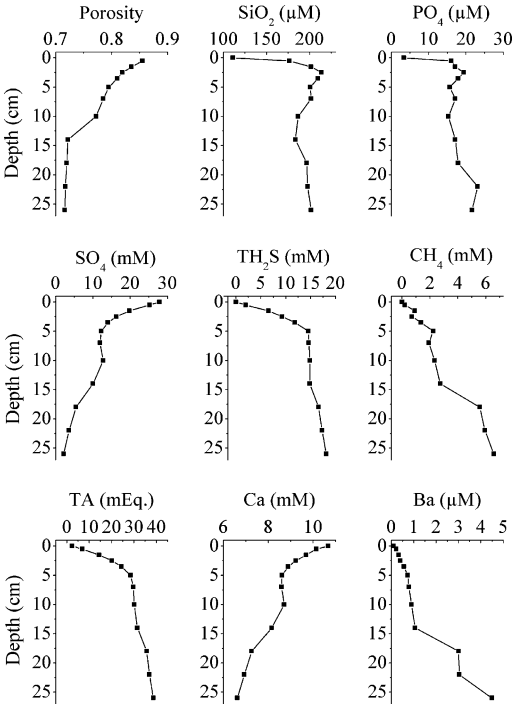

Fig. 4. Porosity and pore water composition in surface sediments covered by bacterial mats (TV-MUC 163-3).

alkalinity values (Figs. 3 and 4). Calcium concentrations are low indicating carbonate precipitation at depth. Sulfate is depleted but not completely consumed at the base of the investigated cores. The presence of both sulfate and methane in millimolar concentrations at the core base is surprising because these chemical species should be converted into sulfide and bicarbonate via microbially-mediated AOM. Sulfide was not removed from the samples prior to sulfate analysis. Thus, some of the detected sulfate might have been produced by sulfide oxidation during sample storage. However, we also measured sulfate in a few additional sub-samples which were acidified and purged with nitrogen gas to remove dissolved sulfide. In these samples we also found millimolar concentrations of sulfate. Thus, we tentatively conclude that the sulfate data reflect in situ values rather than sampling artifacts. A series of gravity cores taken at Mound 12 in areas not affected by fluid venting clearly shows that dissolved sulfate remains close to seawater values in the top few meters of the sediment column while sulfide and methane concentrations are well below 1 mmol and 5 µmol, respectively (Fig. 5). Thus, the thermodynamically unstable composition of the fluids below bacterial mats probably reflects mixing of ambient sulfate-bearing pore waters with sulfate-free and methane-charged fluids ascending from large sediment depths.

3.2. Concentration changes observed in the chamber of the BCL

Bottom waters enclosed in the benthic chambers experienced significant changes over the deployment time of the lander (Figs. 6 and 7). In one particular

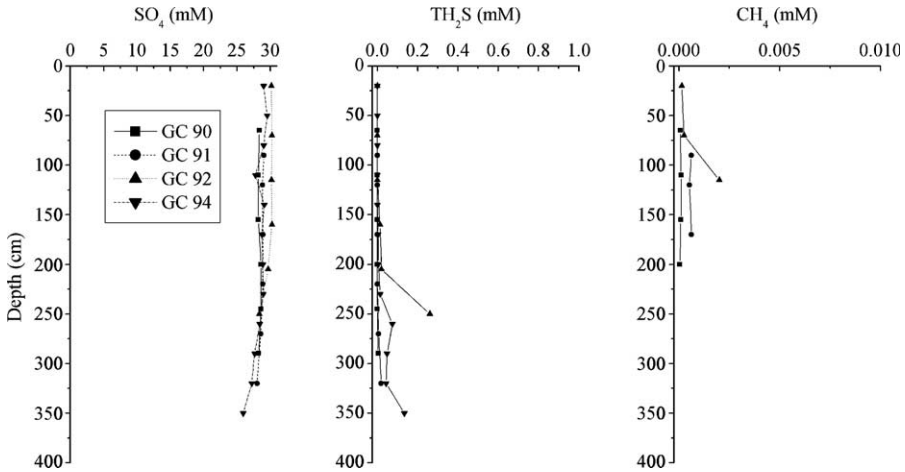

Fig. 5. Dissolved sulfate, sulfide, and methane concentrations in sediments from Mound 12 not affected by fluid venting (GC91 to GC94 in Fig. 2).

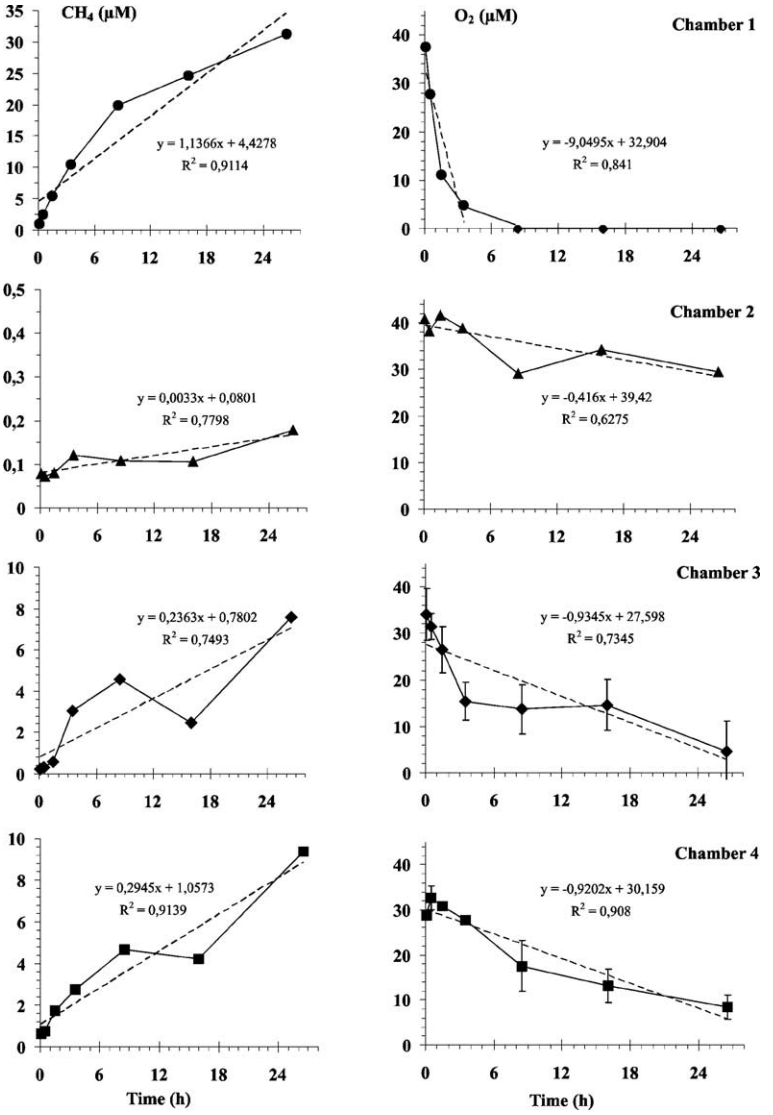

Fig. 6. Changes in methane and oxygen concentration in bottom water enclosed by the 4 benthic chambers. Note the different scales of the methane concentrations. In situ fluxes were calculated by using the slope term of the linear regression. *Due to the strong oxygen consumption in Chamber 1 the linear fit was applied to the first 4 samples containing oxygen.

chamber (no. 1) dissolved oxygen and nitrate declined rapidly and were almost completely consumed within 8 h after the instrument deployment. Dissolved sulfide started to increase after oxygen and nitrate were depleted while methane increased immediately upon the instrument's deployment. Total alkalinity increased rapidly over the first 3 h of the measurement and more slowly towards the end of the deployment. Dissolved silica was enhanced soon after the instrument was placed at the seafloor and showed only a very slow increase during the following hours. Dissolved manganese, phosphate and barium remained close to seawater values until oxygen was strongly depleted. The behavior of manganese and phosphate is probably related to the reductive dissolution of metal oxides inducing the release of Mn and phosphate previously adsorbed on manganese and iron oxides and hydroxides and thus may be

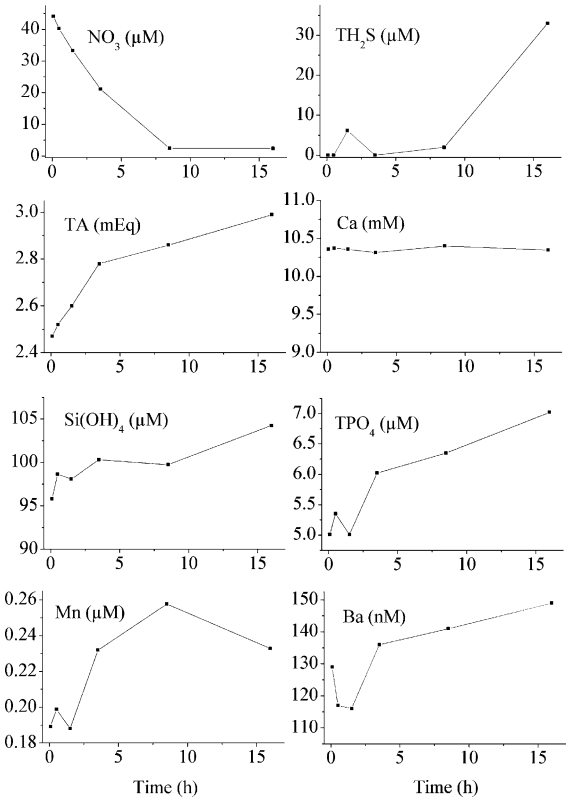

Fig. 7. Changes in dissolved species concentrations in bottom water enclosed by Chamber 1. The concentrations of major seawater ions (Na, Mg, Ca, Cl, SO_4) remained constant over time (calcium data shown as example).

largely an artifact. The similar behavior of barium is surprising because Ba-cycling is believed to be controlled by the precipitation of barite ($BaSO_4$) and the prevailing sulfate concentration which did not change over the deployment time. Possibly, oxygen depletion inhibited further sulfate production via sulfide oxidation so that the local concentration of dissolved sulfate in microbially active microenvironments was depleted by the changing redox conditions favoring the late release of dissolved barium. Concentrations of dissolved sulfate and calcium in the chamber water might have changed as well. However, the measured concentrations were constant within the precision of the applied analytical methods (1–2% relative standard deviation for three replicates) because of the high background concentrations of these ions in seawater. Much longer deployment times and/or greater fluid flow velocities would be needed to detect any significant changes in the major ion composition of enclosed bottom waters.

3.3. Model results

Repeated model runs revealed that the best fit to the pore water and benthic chamber data is obtained with a flow velocity of 10 cm yr^{-1} applying the other parameter values listed in Table 1. At higher velocities of upward fluid flow, dissolved sulfide and methane concentrations in the chamber water increase much more rapidly than observed while low flow velocities are not consistent with the sulfate and sulfide pore water data (Fig. 8). Methane concentrations in the millimolar range cannot be measured reliably because methane is lost by degassing into the atmosphere when the samples are retrieved from the seafloor [27]. However, at low methane concentrations (micromolar level) degassing of samples can be avoided when the samples are processed immediately after recovery. Methane concentrations measured in the sediments are thus not correct while the much lower values in the chamber water represent reliable results. The methane concentration at the base of the sediment column was therefore obtained by fitting the model to the methane data measured in the chamber water.

The oxygen concentration in Chamber 1 decreased extremely fast over the first few hours of the deployment (Fig. 6). A rapid initial change is also observed for dissolved silica and total alkalinity (Fig. 7). These changes may be explained by the suspension of sediment particles and pore water upon penetration of the chamber into surface sediments, such that the initial sediment disturbance might have released sulfide and other reducing species, which enhanced the initial oxygen demand. Therefore, the model was not fitted to the rapid changes observed over the first hours but to the more gradual concentration changes occurring in the following period. Also other species that may reduce oxygen were not incorporated in the model reactions.

The benthic oxygen, nitrate, sulfide, and methane fluxes listed in Table 2 are calculated from the change in concentration over time determined in the standard run at time zero (Fig. 8). These fluxes are probably the best estimates for the in situ fluxes at the seafloor prior to the inevitable disturbance induced by the

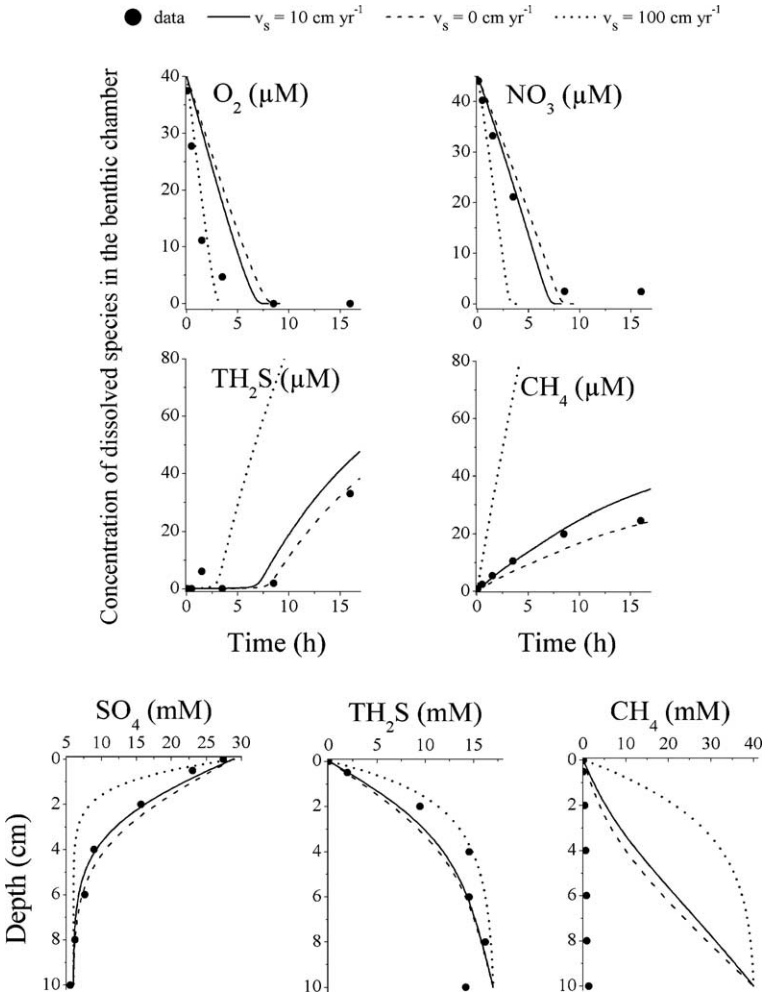

Fig. 8. Model results of Chamber 1. The upper two rows show the temporal change in the composition of the benthic chamber; the lower row depicts the pore water profiles of sulfate, sulfide and methane. Solid dots indicate measured data and lines model results. The best fit to the data was obtained in the standard case and is indicated as solid line (v_S=10 cm yr^{-1}). The model results obtained without upward fluid flow (v_S=0 cm yr^{-1}) are indicated as broken lines while the dotted lines indicate results obtained at high flow velocities (v_S=100 cm yr^{-1}). The other parameters were set to the values of the standard case (Table 1).

lander deployment. They are very close to the oxygen and nitrate fluxes previously calculated for a vent site at Hydrate Ridge (-959 μmol O_2 cm^{-2} yr^{-1} and -767 μmol NO_3^- cm^{-2} yr^{-1} [28].

The dissolved sulfide flux into the benthic chamber column is close to zero as long as dissolved oxygen and nitrate are not completely exhausted (Figs. 6 and 7). In contrast, dissolved methane increases from the very beginning in the presence of dissolved oxygen and nitrate inducing a large in situ flux of methane into the overlying water column (Figs. 6 and 7). Thus, the oxidation of sulfide with oxygen and nitrate is much more efficient than the oxidation of methane (Table 2).

The studied vent site is covered with bacterial mats presumably formed by *Beggiatoa* sp. These microorganisms rely on sulfide as major energy source but are not able to oxidize methane efficiently. It is possible that they consume all oxygen and nitrate inhibiting the spread of other methane-oxidizing microorganisms. In this regard it is instructive to compare the benthic oxygen and nitrate fluxes

Table 2
Oxidation rates, diffusive fluxes (F_{DBL}) and modeled fluxes (F_{MOD}) across the sediment–water interface and at the base of the sediment column (at 10 cm depth) in Chamber 1 compared to measured in situ benthic fluxes of all 4 benthic chambers of BCL 166 (in μmol cm^{-2} yr^{-1})

Benthic Chamber (BC)	BC 1			BC 2	BC 3	BC 4
Species	F_{MOD}	F_{DBL}[a]	Flux[b]	Flux[b]	Flux[b]	Flux[b]
Methane	+440		+139	+0.4	27	28
Methane (at 10 cm sed. depth)	+1032					
Sulfide	+1					
Sulfide (at 10 cm sed. depth)	+238					
Sulfate	−543					
Sulfate (at 10 cm sed. depth)	+45					
Oxygen	−781	−430	−1110	−51	−106	−89
Nitrate	−700	−399				
Dissolved inorganic carbon	+2157					
Reaction	Rate					
Anaerobic oxidation of methane[c]	588					
Aerobic oxidation of sulfide	388					
Sulfide oxidation with nitrate	437					
Aerobic oxidation of methane	4					

Positive flux values indicate fluxes from the sediment into the overlying bottom water while negative values indicate fluxes from the bottom water into the sediments. Oxidation rates and fluxes (F_{MOD}) were derived by modeling pore water and chamber data of Chamber 1 deployed in the centre of an active vent.

[a] Calculated by using the slope term of the linear regression displayed in Fig. 6.

[b] Calculated according to Eq. (17) with a diffusive boundary layer thickness zd of 0.04 cm [21], molecular diffusion coefficients of 430 cm^2 yr^{-1} (O_2) and 355 cm^2 yr^{-1} (NO_3), ambient bottom water concentrations (40 μM O_2 and 45 μM NO_3), and zero concentrations at the interface ($C(0)$=0).

[c] Depth-integrated rate.

calculated in the model with purely diffusive fluxes. These diffusive fluxes (F_{DBL}) can be calculated applying Fick's law to the diffusive boundary layer presumably covering the studied vent site:

$$F_{DBL} = D_M \cdot \frac{C(0) - C_{BW}}{zd}. \quad (17)$$

They result as only −430 μmol O_2 cm^{-2} yr^{-1} and −399 μmol NO_3^- cm^{-2} yr^{-1} (Table 2). As the in situ fluxes calculated from the chamber and pore water data are significantly higher (Table 2), the oxygen and nitrate consuming microorganisms have to rely on additional means to fuel their metabolism with dissolved oxidizing agents. Mat-building *Beggiatoa* spp. are known to form filaments reaching out into the overlying bottom water where plenty of oxygen and nitrate is available. Moreover, they are able to accumulate large amounts of nitrate within their cells [33]. By these means, they can circumvent the diffusive limitation on the oxygen supply in venting fluids. Other microorganisms settling at the seafloor may be left with the presumably very small amount of oxygen and nitrate not consumed by *Beggiatoa* spp. Thus, aerobic methane oxidation at the sediment surface may be inhibited by *Beggiatoa* spp. outcompeting methane-oxidizing microorganisms by the more efficient use of oxygen and nitrate.

The depth-integrated rate of anaerobic methane oxidation is rather small (Table 2) when compared to the rates found at Hydrate Ridge (925 μmol cm^{-2} yr^{-1}; [28]). This is mainly due to the lower methane concentration at the base of the model column (40 mM compared to 68 mM; [29]). Possibly, much of the methane originally dissolved in the rising fluids is already oxidized in the subsurface where the fluids were mixed with sulfate-bearing ambient pore waters (Fig. 3). A significant fraction of the dissolved sulfide and alkalinity entering the surface sediments from below might thus have been formed in a deeper AOM zone underlying the studied surface sediments. Another explanation for the smaller AOM rates are the small growth rates of the AOM communities [20].

Given that no significant amounts of authigenic carbonate are found at the sample site (see Fig. 2), it may be possible that the sampled area has only received a significant methane flux in recent times and that the required microbial biomass to carry out AOM at maximum rate has not sufficiently built up.

Total dissolved inorganic carbon (TCO_2) concentrations in the benthic chamber were calculated from the total alkalinity data using the pH of ambient bottom waters (7.41) and the stability constants recommended by Zeebe and Wolf-Gladrow [34]. The contribution of dissolved sulfide to the total alkalinity was also considered in these calculations. The last three data points were used to determine the benthic flux of TCO_2 because the later phase of the deployment is probably less affected by the emplacement of the benthic chamber (Fig. 9). The resulting flux (Table 2) is much higher than the corresponding methane flux indicating that the total benthic carbon fluxes are dominated by TCO_2.

3.4. Variability and spatial heterogeneity of benthic fluxes

The biogeochemical reactions at the sediment–water interface are stimulated by the injection of reduced chemical species, i.e. methane, hydrogen sulfide. Their oxidation requires oxygen that far exceeds the consumption normally recorded at the deep-sea floor [35]. Whereas the results discussed above are derived from data from one of the four chambers, the varying pore water composition (in Chamber 4) and concentration changes over time in the remaining three chambers of the same lander deployment clearly show the scale and venting heterogeneity in these sediments. Different visible appearance, colonisation pattern and pore water composition occur over distances of 40 cm. Whereas Chamber 1 had an almost complete coverage by bacterial mats and recorded the highest fluxes; sediments in Chamber 2 appeared not affected by venting as the chamber data show small concentration changes in oxygen and methane over time (Fig. 6) resulting in benthic fluxes of 51 and 0.4 μmol cm^{-2} yr^{-1}, respectively (Table 2). Compared to this, the enclosed bottom water in Chambers 3 and 4 containing sediments with a slight coverage by bacterial mats and dorvelliid polychaetes experienced an intermediate flux of methane and oxygen consumption during the 26.5 h of deployment. This is reflected as well in the direct comparison of the pore water composition of Chambers 1 and 4 (Fig. 3). Major differences are found for SO_4 which reaches minimum concentrations of <5 mM in Chamber 1 compared to 24.5 mM in Chamber 4. Similar dramatic differences are revealed for TH_2S and TA which imply remarkable differences in fluxes on a decimeter scale.

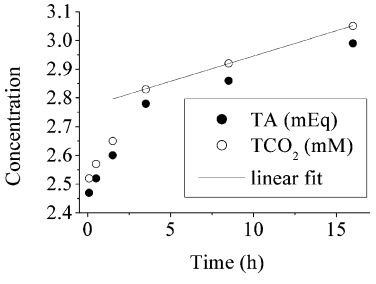

Fig. 9. Change in total alkalinity (TA) and total dissolved inorganic carbon (TCO_2) in Chamber 1. The linear fit was applied to the last three TCO_2 data points.

4. Conclusions

In situ measurements with chambers placed at the seafloor have to be evaluated carefully to avoid erroneous results. Thus, concentration changes recorded immediately after the deployment of the instrument may be too high because of the disturbance and suspension of surface sediments. Moreover, fluxes of reduced chemicals (sulfide, methane) depend on the concentration of dissolved oxygen in the chamber water. As oxygen is rapidly depleted during the deployment, the flux data recorded towards the end of the deployment may also be erroneous. These artifacts may be avoided by improving the design of the instrument. Thus, a gas exchange system was developed to compensate for the oxygen consumption of the enclosed sediment community [36]. Here, we took an alternative approach using the ability of our lander system to recover also the incubated surface sediments. We developed and applied a new numerical model to evaluate both chamber and pore water data. With this approach, we were able to derive in situ benthic flux data which are much better constrained and more reliable than previous estimates.

In the centre of an active vent investigated in our study methane-charged fluids ascend to the surface. About 57% of the inflowing methane is consumed within the surface sediments by the anaerobic oxidation of methane while less than 1% is oxidized at the sediment surface by aerobic microorganism using oxygen as terminal electron acceptor. The poor efficiency of aerobic methane oxidation may be caused by the limited availability of oxygen at the sediment–water interface. The studied sediments were covered with a bacterial mat presumably formed by sulfide-oxidizing microorganisms. These organisms probably consumed most of the available oxygen suppressing the activity of methane-oxidizing microorganisms. As many active vent sites are covered by mats of sulfide-oxidizing bacteria, aerobic methane oxidation may also be inhibited at other vent sites. Thus, the flux of methane into the overlying bottom waters may be regulated by anaerobic rather than aerobic methane oxidation.

Our measurements revealed an extreme heterogeneity of benthic fluxes over a lateral distance of only 40 cm. They imply that fluid flow is focused to small active vents with a diameter of a few decimeters or even less. The extreme focusing of fluid flow has to be considered when active structures such as mud diapirs are investigated to determine rates of fluid flow and fluxes of dissolved species at the sediment–water interface.

Acknowledgements

Many thanks are due to the vessel's master Hening Papenhagen and crew of *R/V Meteor*. Without the dedication and support of Bernhard Bannert, Michael Poser, Wolfgang Queisser and Matthias Türk, the deployment and functioning of our equipment would not have been possible. We are grateful for the analytical work of Bettina Domeyer, Karen Stange, Kristin Nass and Anke Bleyer at sea and in the shore-based laboratory. We appreciate the help of Christine Utecht in improving the figures and thank the reviewers, Marta E. Torres and Ralf Haese, for their helpful comments and suggestions to improve the manuscript. The cruise was supported by the Deutsche Forschungsgemeinschaft as part of the Sonderforschungsbereich (SFB) 574 ("Volatiles and Fluids in Subduction Zones: Climate Feedback and Trigger Mechanisms for Natural Disasters"); this is SFB 574-contribution Nr. 51.

References

[1] J.C. Moore, P. Vrolijk, Fluids in accretionary prisms, Rev. Geophys. 30 (1992) 113–135.
[2] A.J. Kopf, Significance of mud volcanism, Rev. Geophys. 40 (2002) 1005, doi:10.1029/2000RG000093.
[3] A.V. Milkov, Worldwide distribution of submarine mud volcanoes and associated gas hydrates, Mar. Geol. 167 (2000) 29–42.
[4] M.J. Mottl, Pore waters from serpentinite seamounts in the Mariana and Izu-Bonin forearcs, Leg 125: evidence for volatiles from the subducting slap, Sci. Results, vol. 125, Ocean Drilling Program, 1992, pp. 373–385.
[5] K.M. Brown, The nature and hydrogeologic significance of mud diapirs and diatremes for accretionary system, J. Geophys. Res. 95 (1990) 8969–8982.
[6] P. Henry, X.L. Pichon, S. Lallemant, S. Lance, J. Martin, J.-P. Foucher, A. Fiala-Médioni, F. Rostek, N. Guilhaumou, V. Pranal, M. Castrec, Fluid flow in and around a mud volcano field seaward of the Barbados accretionary wedge: results from Manon cruise, J. Geophys. Res. 101 (1996) 20297–20323.
[7] A. Kopf, D. Klaeschen, J. Mascle, Extreme efficiency of mud volcanism in dewatering accretionary prisms, Earth Planet. Sci. Lett. 189 (2001) 295–313.
[8] M. Wiedicke, H. Sahling, G. Delisle, E. Faber, S. Neben, H. Beiersdorf, V. Marchig, W. Weiss, N.v. Mirbach, A. Afiat, Characteristics of an active vent in the fore-arc basin of the Sunda arc, Indonesia, Mar. Geol. 184 (2002) 121–141.
[9] T.H. Shipley, K.D. McIntosh, E.A. Silver, P.L. Stoffa, Three-dimensional seismic imaging of the Costa Rica accretionary prism: structural diversity in a small volume of the lower slope, J. Geophys. Res. 97 (1992) 4439–4459.
[10] L.M. Kahn, E.A. Silver, D. Orange, R. Kochevar, B. McAdoo, Surficial evidence of fluid expulsion from the Costa Rica accretionary prism, Geophys. Res. Lett. 23 (1996) 887–890.
[11] E. Zuleger, J.M. Gieskes, C.-F. You, Interstitial water chemistry of sediments of the Costa Rica accretionary complex off the Nicoya Peninsula, Geophys. Res. Lett. 23 (1996) 899–902.
[12] G. Bohrmann, E. Suess, J. Geinert, B. Teichert, T. Naehr, Gas hydrate carbonates from Hydrate Ridge, Cascadia Convergent Margin: indicators of near-seafloor clathrate deposits, Fourth International Conference on Gas Hydrates, Yokohama, 2002.
[13] E. Soeding, K. Wallmann, E. Suess, E. Flueh, RV METEOR, Cruise Report M54/2+3. Fluids and Subduction, Costa Rica 2002, p. 366, GEOMAR Report 111, 2003.
[14] T. Moerz, A. Kopf, W. Brueckmann, H. Sahling, N. Fekete, V. Huenerbach, D. Masson, D.A. Hepp, E. Suess, Styles and productivity of mud diapirism along the Middle American Margin: Part I. Margin evolution, segmentation, dewatering and mud diapirism, in: G. Martinelli, B. Panahi (Eds.), Mud

Volcanoes, Geodynamics and Seismicity, NATO Sci. Ser. IV, Springer, Dordrecht, 2005, pp. 35–48.
[15] X. Han, E. Suess, H. Sahling, K. Wallmann, Fluid venting activity on the Costa Rica margin: new results from authigenic carbonates, Int. J. Earth Sci. (Geol. Rundschau) 93 (2004) 596–611, doi:10.1007/s00531-004-0402-y.
[16] C. Hensen, K. Wallmann, M. Schmidt, C.R. Ranero, E. Suess, Fluid expulsion related to mud extrusion off Costa Rica—a window to the subducting slab, Geology 32 (2004) 201–204.
[17] S. Mau, H. Sahling, G. Rehder, E. Suess, P. Linke, E. Soeding, Estimates of methane output from mud extrusions at the erosive convergent margin off Costa Rica, Mar. Geol., submitted for publication.
[18] T. Moerz, N. Fekete, A. Kopf, W. Brueckmann, S. Kreiter, V. Huenerbach, D. Masson, D.A. Hepp, M. Schmidt, S. Kutterolf, H. Sahling, F. Abegg, V. Spiess, E. Suess, C.R. Ranero, Styles and productivity of mud diapirism along the Middle American Margin: Part II. Mound Culebra and Mounds 11 and 12, in: G. Martinelli, B. Panahi (Eds.), Mud Volcanoes, Geodynamics and Seismicity, NATO Sci. Ser. IV, Springer, Dordrecht, 2005, pp. 49–76.
[19] H. Sahling, D. Rickert, R.W. Lee, P. Linke, E. Suess, Macrofaunal community structure and sulfide flux at gas hydrate deposits from the Cascadia convergent margin, Mar. Ecol., Prog. Ser. 231 (2002) 121–138.
[20] A. Boetius, E. Suess, Hydrate Ridge: a natural laboratory for the study of microbial life fueled by methane from near-surface gas hydrates, Chem. Geol. (2004) 291–310.
[21] U. Witte, O. Pfannkuche, High rates of benthic carbon remineralisation in the abyssal Arabian Sea, Deep-Sea Res. 47 (2000) 2785–2804.
[22] O. Pfannkuche, P. Linke, GEOMAR Landers as long-term deep-sea observatories, Sea Technol. 44 (2003) 50–55.
[23] C. Niewöhner, C. Hensen, S. Kasten, M. Zabel, H.D. Schulz, Deep sulfate reduction completely mediated by anaerobic methane oxidation in sediments of the upwelling area off Namibia, Geochim. Cosmochim. Acta 62 (1998) 455–464.
[24] K. Grasshoff, L.G. Anderson, Methods of Seawater Analysis, Verlag Chemie, Weinheim, 1999, 600 pp.
[25] V.N. Ivanenkov, Y.I. Lyakhin, Determination of total alkalinity in seawater, in: O.K. Bordovsky, V.N. Ivanenkov (Eds.), Methods of Hydrochemical Investigations in the Ocean, Nauka Publ. House, Moscow, 1978, pp. 110–114.
[26] B.P. Boudreau, A method-of-lines code for carbon and nutrient diagenesis in aquatic sediments, Comput. Geosci. 22 (1996) 479–496.
[27] R. Luff, K. Wallmann, S. Grandel, M. Schlüter, Numerical modelling of benthic processes in the deep Arabian Sea, Deep-Sea Res. 47 (2000) 3039–3072.
[28] R. Luff, K. Wallmann, Fluid flow, methane fluxes, carbonate precipitation and biogeochemical turnover in gas hydrate-bearing sediments at Hydrate Ridge, Cascadia Margin: numerical modeling and mass balances, Geochim. Cosmochim. Acta 67 (2003) 3403–3421.
[29] T. Treude, A. Boetius, K. Knittel, K. Wallmann, B.B. Jørgensen, Anaerobic oxidation of methane above gas hydrates (Hydrate Ridge, OR), Mar. Ecol. Prog. Ser. 264 (2003) 1–14.
[30] B.P. Boudreau, Diagenetic Models and their Implementations, Springer, New York, 1997, 116 pp.
[31] A. Boetius, K. Ravenschlag, C.J. Schubert, D. Rickert, F. Widdel, A. Gieseke, R. Amann, B.B. Jørgensen, U. Witte, O. Pfannkuche, A marine microbial consortium apparently mediating anaerobic oxidation of methane, Nature 407 (2000) 623–626.
[32] E. Suess, M.J. Whiticar, Methane-derived CO_2 in pore fluids expelled from the Oregon subduction zone, Palaeogeogr. Palaeoclimatol. Palaeoecol. 71 (1989) 119–136.
[33] S.C. McHatton, J.P. Barry, H.W. Jannasch, D.C. Nelson, High nitrate concentrations in vacuolate, autotrophic marine *Beggiatoa* spp, Appl. Environ. Microbiol. 62 (1996) 954–958.
[34] R. Zeebe, D. Wolf-Gladrow, CO_2 in Seawater: Equilibrium, Kinetics and Isotopes, Elsevier, Amsterdam, 2001, 346 pp.
[35] E. Suess, M.E. Torres, G. Bohrmann, R.W. Collier, J. Greinert, P. Linke, G. Rehder, A. Trehu, K. Wallmann, G. Winckler, E. Zuleger, Gas hydrate destabilization: enhanced dewatering, benthic material turnover and large methane plumes at the Cascadia convergent margin, Earth Planet. Sci. Lett. 170 (1999) 1–15.
[36] S. Sommer, O. Pfannkuche, P. Linke, R. Luff, J. Greinert, M. Drews, S. Gubsch, M. Pieper, M. Poser, W. Queisser, A. Petersen, The efficiency of the benthic filterbiological control of the emission of dissolved methane from sediments hosting shallow gas hydrates at Hydrate Ridge, Glob. Biogeochem. Cycles, submitted for publication.